



**HAL**  
open science

# Radiative and microphysical interactions between marine stratocumulus clouds and Saharan dust 2. Modeling

F. Pradelle, Guy Cautenet, I. Jankowiak

► **To cite this version:**

F. Pradelle, Guy Cautenet, I. Jankowiak. Radiative and microphysical interactions between marine stratocumulus clouds and Saharan dust 2. Modeling. *Journal of Geophysical Research*, 2002, 107 (D19), 10.1029/2000JD000156 . hal-02077101

**HAL Id: hal-02077101**

**<https://uca.hal.science/hal-02077101>**

Submitted on 27 Jan 2021

**HAL** is a multi-disciplinary open access archive for the deposit and dissemination of scientific research documents, whether they are published or not. The documents may come from teaching and research institutions in France or abroad, or from public or private research centers.

L'archive ouverte pluridisciplinaire **HAL**, est destinée au dépôt et à la diffusion de documents scientifiques de niveau recherche, publiés ou non, émanant des établissements d'enseignement et de recherche français ou étrangers, des laboratoires publics ou privés.

# Radiative and microphysical interactions between marine stratocumulus clouds and Saharan dust

## 2. Modeling

F. Pradelle and G. Cautenet

Laboratoire de Météorologie Physique, Université Blaise Pascal, Aubière, France

Received 13 November 2000; revised 14 August 2001; accepted 9 October 2001; published 15 October 2002.

[1] In the first part of this study, we attempted to highlight some radiative effects of dust particles in the presence of clouds using satellite observations. A statistical study over 6 years of daily Meteosat images revealed a minimum in the apparent cloud albedo (ocean-cloud-atmosphere system) ranging between 10% and 20%, near the West African coast. These decreases were observed at any season, and over the areas where the dust outbreaks are the most frequent. In order to explain these observations, we begin this second part by radiative simulations using the ECMWF radiative code. It appears that the presence of dust over the cloud cover (i.e., summer configuration) leads to a decrease in albedo of the ocean-cloud-atmosphere system reaching about 15% on average, i.e., a value comparable to the one observed by satellite. In winter, however, dust is found in the trade wind layer, at the same level as the cloud cover, but a simple direct effect (superposition effect) cannot explain the observed albedo decrease. According to earlier experimental studies, dust aging is frequently observed in the atmosphere. Complex interactions involving other particles and chemical species enhance the soluble fraction of dust: in-cloud processing, chemical reactions on dust surface, transfer of small sulfate particles toward the large dust particles. Microphysical simulations using an air parcel model reveal that dust presence in a stratiform cloud field may lead to a decrease in the initial cloud condensation nucleus number, an increase of the effective droplet radius, and eventually, a reduction of the cloud albedo. This albedo decrease may reach more than 10% under certain conditions. On average, the albedo of the system is found to be reduced by a value ranging between 3% and 10%. Simulations performed with a mesoscale model reveal the presence at altitude of carbonaceous particles emitted by the African savanna burning in winter. Dust microphysical effects associated with the presence of absorbent carbonaceous particles at altitude would decrease the system albedo by more than 10% and so would explain the satellite observations during the winter season too in the southern part of the area under study. All these computations are in rather good agreement with the satellite observations and confirm the assumption that dust particles play an important climatic role to the west of the African coast. According to our estimates, the radiative forcing associated with the dust in the presence of clouds is (1) globally always positive along the column and (2) located either near the surface (winter case) or at altitude (summer case) according to the season. In the last case (summer), the radiative forcing remains negative near the surface but will be overcompensated by positive values at altitude (dust level).

*INDEX TERMS:* 0305 Atmospheric Composition and Structure: Aerosols and particles (0345, 4801); 0360 Atmospheric Composition and Structure: Transmission and scattering of radiation; 0320 Atmospheric Composition and Structure: Cloud physics and chemistry; 3374 Meteorology and Atmospheric Dynamics: Tropical meteorology; *KEYWORDS:* dust outbreak, stratiform clouds, microphysical model, mesoscale model, cloud albedo decrease, radiative forcing

**Citation:** Pradelle, F., and G. Cautenet, Radiative and microphysical interactions between marine stratocumulus clouds and Saharan dust, 2, Modeling, *J. Geophys. Res.*, 107(D19), 4413, doi:10.1029/2000JD000156, 2002.

### 1. Introduction

[2] Every year, large amounts of dust particles are vented in the Saharan/Sahelian desert and moved toward the

tropical North Atlantic Ocean over several thousands of kilometers [*Prospero and Nees, 1977; Schütz et al., 1981; Jankowiak and Tanré, 1992*]. *Jankowiak [1992]* showed that in the absence of clouds, dust particles have a significant direct radiative effect (negative forcing) over the ocean. According to the literature [*Chiapello et al., 1995, 1999*],

there are two distinct regimes in the dust transport over the North Atlantic Ocean, depending on the season. During summer, mineral dust travels in the Saharan Air Layer (SAL), above the stratocumulus cover. Both layers are separated by the trade wind temperature inversion. During winter, however, dust particles are mainly found in the Trade Wind Layer (TWL). Thus, during winter, dust particles are either below or inside the clouds.

[3] In order to study a possible effect of dust particles on the “apparent” cloud albedo, i.e., the albedo of the ocean-cloud-dust-atmosphere system, we have developed in part 1 of this study [Pradelle *et al.*, 2002] a numerical algorithm using visible and infrared Meteosat data. This algorithm allowed us to differentiate ocean, dust and cloud pixel signals and to set up a climatology of dust plume location and of the mean apparent cloud albedo during a 6-year period over the northeastern Atlantic Ocean. This statistical study of daily Meteosat images showed a minimum in the apparent cloud albedo near the West African coast for the four months considered in our study (January, April, July and October). A very important result of this analysis is that the apparent cloud albedo decreases over the area where the dust outbreaks are the most frequent. A zonal average of this decrease has been calculated along the West African coast: It ranges between 10% in autumn (near 15°N) and 20% during the spring months (near 10°N). These observations suggested that the dust particles, in the presence of clouds, could lead to a slight positive forcing in solar radiation.

[4] In the present paper, we will attempt to highlight some physical phenomena that give an explanation for the decrease in the apparent cloud albedo observed by satellite measurements. In section 2, we show several radiative simulations in order to assess the direct radiative effect of a dust plume in the presence of stratiform clouds. Various numerical simulations are presented depending on the relative position of the dust plume and the cloud cover, according to the seasonal features of the dust particles transport. The main purpose of these simulations is to verify if the apparent cloud albedo decrease can be explained by a simple radiative direct effect only.

[5] In a second part (section 3), we use a microphysical model to investigate the mixing of dust particles with water droplets in a winter case (when dust is found in the TWL, i.e., in the same level as the major part of the clouds). According to Levin *et al.* [1996] and Wurzler *et al.* [2000], dust particles could interact with salt and sulfate particles, which serve as cloud condensation nuclei (CCN), and therefore can change the size of cloud droplets. We study the possible modifications of the droplet distribution and assess the subsequent change of the stratiform cloud albedo. We compare with the satellite observations and attempt to quantify this indirect effect.

[6] Section 4 summarizes the different radiative phenomena that dust particles can induce in the presence of clouds, and depending on the season, we attempt to explain the satellite observations. As in January, black carbon aerosol (BC) from bush fires could a priori radiatively interact with clouds; it was necessary to get an order of magnitude of the radiative effect of these particles: This was performed using the RAMS model coupled with an emission scheme for biomass burning based on satellite measurements.

## 2. Radiative Modeling and Direct Effects Simulations

[7] Before studying the complex microphysical interactions between dust particles and water droplets, we first have to assess the direct radiative effect of a dust plume in the presence of clouds over the ocean. The aim of this preliminary task is to investigate the possibility that the decrease in apparent cloud albedo as observed by satellite could be due to a simple superposition of clouds and the dust layer. First, we briefly present the radiative model used here.

### 2.1. Radiative Code

[8] We use the radiative code based on the European Centre for Medium-Range Weather Forecasts (ECMWF) radiative model, in its “EC3” version [Morcrette and Fouquart, 1986; Morcrette, 1989]. It is derived from previous high-resolution models developed at the Laboratoire d’Optique Atmosphérique (LOA) [Fouquart and Bonnel, 1980; Morcrette and Fouquart, 1986; Morcrette *et al.*, 1986; Frouin *et al.*, 1986]. This version is weakly CPU consuming, while it remains quite accurate, according to the tests of the Inter-comparison of Radiation Codes for Climate Models (IRCCM) [Fouquart *et al.*, 1991]. In the solar band (SW band), fluxes are computed using a “two stream” approximation [Fouquart and Bonnel, 1980] on four wavelength intervals (six in the longwave part of the spectrum). The four SW intervals are as follows: [0.25  $\mu\text{m}$  to 0.69  $\mu\text{m}$ ], [0.69  $\mu\text{m}$  to 1.19  $\mu\text{m}$ ], [1.19  $\mu\text{m}$  to 2.38  $\mu\text{m}$ ] and [2.38  $\mu\text{m}$  to 4  $\mu\text{m}$ ]. The gaseous absorption coefficients ( $\text{H}_2\text{O}$ ,  $\text{CO}_2$  and  $\text{O}_3$ ) are derived from the Air Force Geophysics Laboratory (AFGL) compilation of coefficients, and the dependence on the pressure and the temperature is based upon a parameterization described by Morcrette *et al.* [1986]. We use the standard tropical atmosphere given by McClatchey *et al.* [1973], distributed on 36 vertical layers centered on 36 pressure levels (from 1010 to 10 hPa). The code has been modified [Chomette, 1999] in order to take the particular radiative properties of the mineral dust particles into account. These properties have been derived from Mie calculations, using size distributions and refractive index given by Alfaro *et al.* [1998] and d’Almeida *et al.* [1991], respectively.

[9] The model inputs are the 550 nm aerosol optical thickness and the liquid water content (LWC) at each level, along with the effective radius of the cloud droplets. The visible reflectivity of the surface is also required. In the output of the model we get the outgoing shortwave (SW) radiative flux and therefore the albedo that we can compare to the satellite measurements.

### 2.2. Radiative Simulations

#### 2.2.1. Initial Conditions

[10] In our radiative simulations, the visible reflectivity of the ocean surface is taken equal to 0.05, according to the satellite measurements [Pradelle *et al.*, 2002]. We study a typical stratiform cloud developing between the levels 920 and 905 hPa (i.e., about 150 m thick) in the cloud layer, top of the TWL (near 1000 m in altitude). The effective radius of the droplets and the LWC are taken constant and equal to 7  $\mu\text{m}$  and 0.4  $\text{g kg}^{-1}$ , respectively, according to Martin *et al.* [1993]. These properties result in an apparent cloud albedo  $\alpha_0$  (system surface-cloud-atmosphere, without dust par-

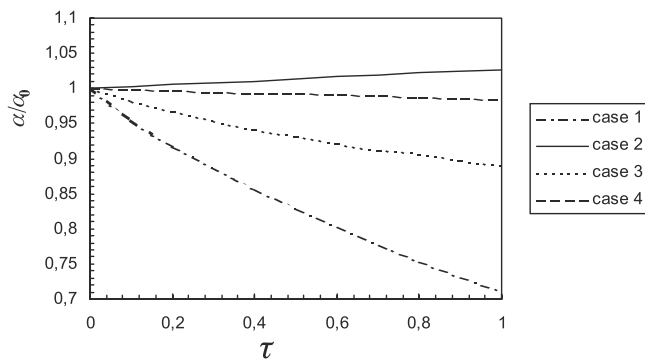


**Figure 1.** Direct radiative effect of the dust layer on the surface-cloud-atmosphere system. The results are expressed in terms of albedo  $\alpha$  normalized by the albedo computed without dust  $\alpha_0$ , against the dust layer optical thickness. Case 1: the dust plume is lying clearly above the cloud cover; case 2: dust is lying below the cloud; case 3: the dust layer is at the same level as the cloud; case 4: the dust fills the atmosphere from the surface up to the top of the cloud.

ticles) of 0.45. This value is close to the average value of the apparent albedo of the “warm” clouds measured in the outbreak areas by satellite radiometers in the first part of this study.

[11] Four different scenarios will be considered in this section, corresponding to four different relative positions of the dust and the cloud layers, while the position of the stratocumulus remains unchanged. Case 1 corresponds to a superposition of the cloud and the dust plume: The dust layer is above the cloud cover, in the SAL, between the levels 700 and 600 hPa (i.e., between about 3000 and 4000 m). In case 2, the dust plume is below the cloud, in the TWL, between surface and the 930 hPa level. In case 3, the dust plume is at the same level as the cloud, i.e., between the levels 920 and 905 hPa. Finally, in case 4, the dust plume fills all the TWL, from surface up to the top of the cloud. Note that in cases 3 and 4, only the direct radiative effects are considered. In this section we assume that there are no microphysical interactions between the aerosol particles and the clouds (which are studied in section 3).

### 2.2.2. Results

[12] Figure 1 displays the albedo of the surface-cloud-atmosphere system against the optical depth  $\tau$  of the dust layer for all scenarios. The vertical extension of the dust layer remains constant for each case, and the increase in optical depth corresponds to an increase of the particles concentration, uniformly distributed over the vertical levels considered. The apparent cloud albedo  $\alpha$  is normalized by the albedo  $\alpha_0$  computed without dust. In case 1, the albedo decreases when the optical depth of the dust layer increases, due to the weak but nonnegligible absorptivity of dust particles in the solar band [Chomette, 1999]. This decrease reaches almost 17% for an optical thickness  $\tau = 0.5$ , and 29% for  $\tau = 1$ . Conversely, in case 2, when the dust layer is below the cloud, the albedo very slightly increases. The ratio  $\alpha/\alpha_0$  reaches 1.03 for a dust optical thickness equal to the unity. For case 3,  $\alpha/\alpha_0$  slightly decreases, so as to reach 0.89 for  $\tau = 1$ . Finally, in case 4, there is almost no effect: Even for a dust optical depth equal to 1, the albedo decreases by only 1%. The general trend of these different

results is that the presence of dust over the cloud cover tends to decrease the albedo of the system, due to the slight dust absorptivity in the solar band. However, when dust lies below the cloud cover, the effect becomes negligible. For all clouds thicker than the cloud of our example, this effect will probably disappear completely. In our case, a typical stratocumulus cloud with 200 m thickness, the presence of the dust layer leads to a very slight increase in the albedo of the system. Finally, if the dust plume is found at the same level as the cloud (dust particles are assumed to be in an interstitial phase, without interaction with water droplets), the albedo of the system slightly decreases, due to the slight absorptivity of the dust particles.

[13] As already mentioned above, in summer, dust plumes travel in the Saharan Air Layer (SAL), above the trade winds inversion, i.e., above the cloud cover. Therefore this configuration corresponds to the previous case 1. In winter, however, dust particles are mainly found in the TWL from the ocean surface to the top of the cloud cover [Chiapello *et al.*, 1995]. This configuration corresponds to case 4. Our different results show that the decrease in the cloud albedo observed by satellite in summer could be explained by the presence of a dust layer over the cloud cover. Indeed, the measurements showed that during the summer season, the zonally averaged apparent cloud albedo decreased by about 15% between 15°N to 28°N, along the western tropical African coast. Over this area, the zonally averaged dust optical depth ranges between 0.4 and 0.5 [Husar *et al.*, 1997; Guelle, 1998]. For such an optical thickness, our simulations (Figure 1, case 1) show that the apparent cloud albedo decreases by a value slightly greater than 15%, which corresponds quite well to the satellite observations.

[14] In Figure 2, the ratio  $\alpha/\alpha_0$  is plotted against the cloud LWC, for a constant optical thickness of the dust layer  $\tau$  equal to 0.5. Two curves are plotted, for cases 1 and 4, hereafter referred to as “summer” and “winter” cases, respectively. For the summer case (solid line), we see that for typical LWC values (between 0.3 and 0.8 g kg<sup>-1</sup>), the decrease in the initial albedo is almost constant (between 15% and 16%). That means that the relative cloud albedo

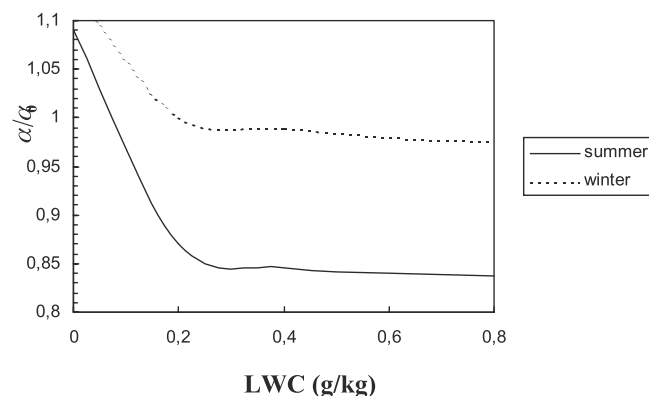


**Figure 2.** Direct radiative effect of the dust layer ( $\tau = 0.5$ ) on the system albedo, depending on the LWC of the cloud. The results are normalized by the albedo computed without dust  $\alpha_0$  and are represented for the summer (solid line) and the winter (dashed line) cases.

decrease does not depend on LWC for most of the clouds. For the winter case, we have observed by satellite (part 1) a relative albedo decrease of 15% also, for a mean dust optical depth greater than 0.4 between 5°N and 10°N. However, our simulations (Figure 1) show that for such a dust optical thickness and in the winter configuration, the very slight decrease in the albedo (about 1%) due to the direct radiative effect of the dust layer is not able to explain the satellite observations. The second curve on Figure 2 (dashed line) confirms that the weak decrease in the cloud albedo simulated in winter is almost independent of the cloud LWC again (for values greater than 0.25 g kg<sup>-1</sup>). This point leads us to investigate other physical processes in order to better understand the effect of a dust layer on the cloud albedo. The next section deals with the possible effects of microphysical interactions between dust particles and liquid water (cloud droplets).

### 3. Microphysical Study

[15] In the previous section, we have seen that in the winter case, the negligible radiative direct effect due to the presence of a dust layer cannot explain the cloud albedo decrease observed by satellite. However, during this season, the dust particles may interact with liquid water droplets of the clouds. Indeed, dust travels in winter in the TWL [Chiapello *et al.*, 1995], where also the major part of the “warm” clouds is located. Microphysical interactions between dust particles and water droplets could lead to a change of the droplet size distribution and therefore to a change of the cloud albedo. It is generally proved that anthropogenic emissions of small particles lead to an increase in cloud albedo [Twomey, 1977; Charlson *et al.*, 1987; Kim and Cess, 1993; Ackerman *et al.*, 1995; Hindman and Bodowski, 1996]. However, dust particles have a larger size, and several studies [Levin *et al.*, 1996; Feingold *et al.*, 1999; Wurzler *et al.*, 2000] have shown that they can act as CCN, increase droplet size and, consequently, decrease the cloud albedo. That could explain, at least in part, our satellite observations. We therefore must investigate the possibility and the implications of such interactions.

#### 3.1. Chemical Properties and Aging of the Dust Particles

[16] Due to their chemical composition, mineral particles should not be hygroscopic in their native state. Wurzler *et al.* [2000] assume that due to their composition, native dust particles could not form droplets. Depending on the geographical origin of the African dust, some differences can be noted in their chemical composition, especially concerning the calcium amount and the ratio Si/Al [Chiapello *et al.*, 1997]. However, Si, Al, and Fe (relatively insoluble materials) are always the main elements composing the Saharan mineral particles [Chiapello *et al.*, 1997; Sokolik and Toon, 1999; Desboeufs *et al.*, 1999]. More soluble elements (Ca, K, Mg and Na) are present in relatively small quantities. Desboeufs *et al.* [1999] have made dissolution experiments on dry segregated loess samples of Saharan origin. By means of an open flow reactor, they measured the soluble fraction of each element after hydration during a typical time for weathering of aerosol particles by cloud water. One of their conclusions is that the dissolution rates are pH-

dependent. In general, there is an increase in the dissolution rates of the dissolved elements as the pH is lowered. For a pH equal to 4.7, typical value for cloud and rainwater [Römer *et al.*, 1985], the average value of the solubility of the whole particles is found equal to 2.1% after 120 min. Desboeufs *et al.* [1999] found the average solubility of the particles to be between about 1% and 4%, depending on the pH. These results confirm the assumption that dust particles, in their native state, would not significantly change the droplet distribution of clouds acting as CCN.

[17] However, the surface of dust particles may be altered in different chemical ways during their long-range transport over the ocean [Zhang, 1994; Song and Carmichael, 1999]. Dust particles are often associated with other relatively soluble species.

[18] Andreae *et al.* [1986] have investigated individual aerosol particles from the remote marine atmosphere. They found that a large fraction of silicate mineral component of the particles was internally mixed with sea salt and excess (non-sea-salt) sulfate. Single-particle analysis on dust collected over the Pacific Ocean, downwind of the Asian coast, showed that 50 to 80% of the large particles (diameter > 2 μm) are coated with sulfate and 50% are coated with nitrate [Parungo *et al.*, 1995]. Measurements in Japan [Horai *et al.*, 1993] show fractions of 5 to 40% of total sulfate mass present on particles larger than 1 μm in diameter. During Kosa events (Japan), half of the sulfate aerosol was present on coarse particle mode [Nishikawa and Kanomari, 1991]. These authors have also found a significant fraction of nitrate on large particles corresponding to the dust particle mode. Concerning the African dust, measurements in Israel [Mamane *et al.*, 1980] reveal that more than 60% of the total sulfate is associated with desert dust during dusty days. Chiapello [1996] shows that more than half of the excess sulfate mass collected at Sal Island (Cape Verde archipelago) may be associated with the coarse mode (dust mode) during some dust events. For significant dust concentrations, sulfates seem to deposit preferentially on dust particles rather than on sea-salt particles. Measurements in the Mediterranean region during June and November 1991 reveal that mineral particles often get coated with sulfate and other soluble materials [Levin *et al.*, 1996]. The amount of soluble material on these particles (sulfate production) is found to be dependent on their surface area. According to these measurements, particles with a diameter of 1 μm have a sulfur fraction (in volume) ranging between about 10% and 15%, depending on the collected samples.

[19] Several studies have attempted to explain these observations and measurements. A detailed microphysical modeling of Wurzler *et al.* [2000] shows that the collection of dust particles by droplets initially formed on sulfate CCN could be a possible pathway for the formation of dust particles with soluble coating. There are many collection mechanisms [Pruppacher and Klett, 1997]: turbulent and Brownian coagulation, phoresis effects, gravitational impaction. . . These mechanisms could explain the presence of dust particles both in interstitial phase and in the cloud droplets as observed by Levin *et al.* [1996] in clouds. Model results [Wurzler *et al.*, 2000] reveal that after three cycles of cloud processing (evaporation/condensation), the major part of the dust particles are processed and contain soluble material. According to their simulations, such coated par-

ticles may themselves act as CCN and so change the water droplet distribution, leading to the production of large drops in convective clouds. Furthermore, chemical reactions on dry or wetted dust particles could also be quite efficient. Chemical box models including the aerosol have shown that dust particles provide an important surface area for sulfate and nitrate formation. *Zhang* [1994] found that 1.3 to 2.3  $\mu\text{g m}^{-3}$  of nitrate and 1.0 to 25  $\mu\text{g m}^{-3}$  of sulfate are formed in this way on mineral dust particles in East Asia, depending on the model conditions. The sulfate is formed by oxidation of the tropospheric  $\text{SO}_2$ , followed by condensation of  $\text{H}_2\text{SO}_4$  on mineral particles surface. It is shown that for increasing dust concentrations, this process becomes more efficient than the direct nucleation of  $\text{H}_2\text{SO}_4$  into particles. The same can be said for the nitrate formation, involving  $\text{HNO}_3$ ,  $\text{NO}_3$  and  $\text{N}_2\text{O}_5$  species. For specific conditions, this pathway could represent 60–80% of their total formation. *Song and Carmichael* [1999] show that a typical dust load value (about 100  $\mu\text{g m}^{-3}$ ) may lead after only 48 hours and in a relatively polluted oceanic area to the formation of more than 8.5  $\mu\text{g m}^{-3}$  of particulate sulfate and about 0.5  $\mu\text{g m}^{-3}$  of  $\text{NO}_3^-$ . In the same time, they recorded a strong decrease in carbonate ions, reacting with  $\text{H}_2\text{SO}_4$ . Under the same atmospheric conditions, *Zhang* [1994] provided the formation of 11.5  $\mu\text{g m}^{-3}$  of  $\text{SO}_4^{2-}$  after 5 days, for a dust load of 100  $\mu\text{g m}^{-3}$  and an initial  $\text{SO}_2$  concentration of 8.0 ppbv. Through sensibility tests he provided the significance of the dust load in this sulfate formation. Thanks to a three-dimensional tropospheric model coupled to a chemistry model, *Dentener et al.* [1996] show the significant role of the mineral aerosol in the tropospheric chemistry at a global scale. According their results, more than 50% of the sulfate is present on mineral dust near the West African coast in annual average, and more than 60% is present during the February-March-April months. They show also that more than 90% of  $\text{HNO}_3$  is associated with dust particles.

[20] All these experiments and model results show that the dust particles are chemically very active, that the chemical composition of the particles can significantly change (aging process of the dust) and that the soluble fraction of the mineral aerosol may become significant far from the sources. *Eichel et al.* [1996] show the important role of the water-soluble fraction of aerosols acting as CCN on the cloud droplet distribution. Through a first in-cloud processing, the preliminary dissolution described by *Desboeufs et al.* [1999] could lead to a first coating of the particle surface with its own dissolved fraction. This coating should obviously change the surface properties of the dust particle. Second, either by cloud processing or by chemical reaction on their surface, dust particles become coated with several soluble species. According to the measurements mentioned above, the soluble fraction of the dust could easily exceed 10% on average, and even more for some particle sizes. This feature is very important, because dust particles could then act as CCN and have a large impact on cloud droplet distribution and, consequently, on the cloud albedo.

## 3.2. Microphysical Simulations

### 3.2.1. Model Description

[21] In order to investigate the indirect radiative effect induced by the microphysical interactions between dust

particles and water droplets, we have used a model composed of three different modules.

[22] The first one is a dynamical module, which is a detailed three-dimensional cloud model developed by *Clark* [1977, 1979]. The use of a vertical stretched grid allows a very high resolution (10–15 m) of the cloud layer and the trade wind inversion. The horizontal grid is 160 m in x and y.

[23] Embedded into trajectories calculated from the simulated 3-D wind field, a Lagrangian parcel model is launched, which includes the spectral microphysical model ExMix. This model was developed by *Wobrock* [1988] in order to study the growth of externally mixed condensation nuclei in fog and clouds. It allows one continuously to follow the individual activated aerosol particles through the droplet spectrum as it considers only one number density distribution function for all aerosol particles and droplets together. The information on the aerosol nucleus and the attached water mass is followed via two different coordinates. In order to take into account the different aerosol types (external mixing), a third coordinate for the chemical composition is added. Each aerosol type differs by its solubility fraction  $\epsilon$ , its dry density  $\rho$ , its molecular weight  $M$ , and its number of free ions  $\nu$ . The advantage of ExMix is that we can attribute to each aerosol particle a different chemical composition, and its growth by condensation to form a drop is correctly calculated. More details of the code and comparisons of simulations with results of field experiments are given by *Schell et al.* [1997] and *Gérémy et al.* [2000].

[24] Finally, the radiative code described in section 2.1 will be used in order to compute the albedo of the system containing the cloud simulated by the two previous modules.

### 3.2.2. Initial Conditions

[25] The aim of this study is to compare the droplet distribution and the albedo of a simulated cloud, with and without the presence of dust particles in the initial aerosol spectrum. The initialization of the dynamical model is made using aircraft measurements performed during the ACE-2 CLOUDYCOLUMN experiment in June–July 1997 [*Brennguier et al.*, 2000]. The flights have been made about 100 km north of Tenerife Island (Canaries archipelago), i.e., in a typical tropical atmosphere. July 9 has been retained here, a day when a nonprecipitating stratocumulus cover was observed in the TWL. Profiles of temperature, humidity and wind up to 5000 m were available from aircraft measurements in order to initialize the cloud model. For the higher levels, ECMWF data were used.

[26] The initial aerosol distribution is derived from measurements (size distributions, properties and chemical compositions) performed at Tenerife during July 1997 in the framework of ACE-2 HILLCLOUD [*Bower et al.*, 2000]. The distribution that we have retained is formed of fine organic particles (mode 1), two modes of non-sea-salt sulfate (advected and processed neutralized sulfuric acid), and a large mode of sea salt (mode 4). The number of sulfate and sea-salt particles is adjusted according to the mass load values generally encountered in the lower layers, west of the African coast. Some of these values are reported in Table 1. The mass of total sulfate and of sea salts is taken equal to 2.5  $\mu\text{g m}^{-3}$  and 4.9  $\mu\text{g m}^{-3}$ , respectively. Table 2 summarizes the characteristics of the initial distribution and

**Table 1.** Some References of nss Sulfate and Sea-Salt Concentration Measurements Over the Tropical Northeastern Atlantic

	P. del Hidalgo, pre-ACE campaign, July 1994	Taganana, ACE-2 HILLCLOUD, July 1997 [Bower <i>et al.</i> , 2000]	Sal Island, December 1994 to February 1995 [Chiapello <i>et al.</i> , 1999]	Sal Island, Winter 1992–1994 [Chiapello, 1996]	Sal Island, Summer 1992–1994 [Chiapello, 1996]	Eumeli 3 Cruise, September– October 1991 (18.5°N, 21.2°W) [Putaud <i>et al.</i> , 1993]	Eumeli 3 Cruise, September– October 1991 (25.4°N, 16.6°W) [Putaud <i>et al.</i> , 1993]
nss SO <sub>4</sub> <sup>2-</sup> , μg m <sup>-3</sup>	2.43	1.2	2.5	1.9	2.6	2.5	2.8
sea Na <sup>+</sup> , μg m <sup>-3</sup>	2.2	-	5.3	1.7	4	-	-

the chemical properties of the particles (modes 1 to 4). In order to investigate the microphysical role of the mineral particles, a large mode of dust (mode 5) may be added to this distribution and is also described in Table 2. The number concentration of dust particles can be modified from 0 to 153 cm<sup>-3</sup> (i.e., up to 600 μg m<sup>-3</sup>) and their solubility from 1% to 20%. Thus scenarios with or without this dust mode can be studied. Figure 3 represents the initial aerosol distribution (solid line) and an additional mode of dust particles with a loading of 200 μg m<sup>-3</sup> (dashed line).

[27] The effective radius of the cloud droplets and the LWC formed with the ExMix module will then be used in the radiative code in order to calculate the albedo of the system. We assume that the optical properties of the water droplets remain unchanged when they contain dust particles.

### 3.2.3. Results

[28] Among several trajectories computed with the cloud model, we have retained a rising trajectory starting from 750 m (cloud base) and reaching 950 m after about 900 s. Then the trajectory remains horizontal until about  $t = 2000$  s, blocked vertically by the inversion layer (top of the TWL). The microphysics of the cloud are simulated with the ExMix model and evolve in the air parcel driven along this trajectory. In the whole section, the results are given at the time  $t = 1800$  s, a characteristic time for a stratocumulus development. We assume that at this time the droplet distribution is representative of the cloud top distribution. This trajectory is represented in Figure 4.

[29] Figure 5 gives the droplet size distributions formed on the different CCN spectra. In solid lines, the distribution is computed with the initial aerosol distribution (no dust). The other curves are calculated when the dust mode is added, for a dust particles solubility ranging from 1% to 20%. We have made calculations for three dust loads: 200 μg m<sup>-3</sup> (Figure 5a), 400 μg m<sup>-3</sup> (Figure 5b) and 600 μg m<sup>-3</sup> (Figure 5c). First, note that all the distributions are centered on radii ranging from about 6 μm to 8 μm, which

are typical values for the top of a stratocumulus cloud [Martin *et al.*, 1993]. Second, we see that whatever the dust load, the general trend is a decrease and a broadening (with a slight shift toward the large radii) of the droplet spectrum when dust particles are added. Indeed, except for  $\epsilon = 1\%$ , where the maximum of the curve seems slightly enhanced, the increase in solubility leads to a decrease in the maximum on the curve. Finally, we see that for identical values of solubility, the modifications of the droplet distribution described above are more pronounced when the dust load increases (from Figure 5a to Figure 5c). All these conclusions show that dust particles can change the droplet distribution of a tropical stratocumulus if they contain soluble material. Now we have to assess more accurately the influence of the dust on the cloud optical properties.

[30] The evolution of the effective radius  $r_e$  of the droplets against the dust concentration is represented in Figure 6a. This radius is defined as the ratio of the third to the second moment of the size spectrum:

$$r_e = \frac{\int_{r=0}^{\infty} N(r)r^3 dr}{\int_{r=0}^{\infty} N(r)r^2 dr}$$

where  $r$  is the cloud droplet radius and  $N(r)$  is the spectral droplet concentration. The results are expressed in terms of effective radius normalized by the effective radius  $r_{e0}$  computed without dust, for four different solubilities. At  $t = 1800$  s, we have  $r_{e0} = 7.4$  μm. We see that for a dust particles solubility of 1%, the rise of the mineral aerosol concentration leads to a slight decrease in the effective radius. The effective radius decreases by about 2% for a dust mass concentration of 600 μg m<sup>-3</sup>. However, for all the other values of solubility, the addition of dust particles leads to an increase in the effective droplet radius. The higher the solubility and the concentration, the stronger the increase in effective radius. The ratio  $r_e/r_{e0}$  exceeds 1.14 for  $\epsilon = 20\%$

**Table 2.** Aerosol Distribution Used as Input in the Microphysical ExMix Model<sup>a</sup>

	$N$	$d$	$\sigma$	$m$	$\rho$	$M$	$\nu$	$\epsilon$
<i>Initial Distribution</i>								
Mode 1, organic particles	280	12	1.9	0.003	1.3	200	3	0.5
Mode 2, nss sulfate 1	400	70	1.45	0.35	1.8	120	2	0.7
Mode 3, nss sulfate 2	250	140	1.6	2.15	1.7	140	4	0.6
Mode 4, sea salt	6	640	1.8	4.9	2	60	3	0.9
<i>Additional Mode</i>								
Mode 5, dust	51/153	1140	1.53	200/600	2.65	420	2	0.01/0.3

<sup>a</sup> These values are derived from the ACE-2 HILLCLOUD campaign. The initial distribution is composed of four modes. A fifth mode (mode 5) of dust particles may be added. For each mode the distribution characteristics and the chemical properties of the particles are mentioned: the total number of particles  $N$ , the median diameter  $d$  and the standard deviation  $\sigma$  of the lognormal distribution, the total mass of particles  $m$ , their dry density  $\rho$ , the molecular weight  $M$ , the number of free ions  $\nu$  and the solubility fraction  $\epsilon$ .

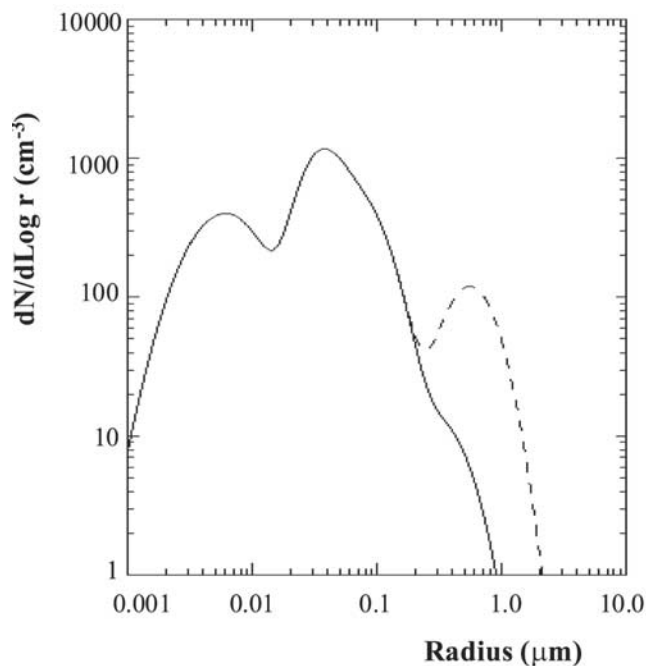


**Figure 3.** Size distribution of the initial dry aerosol spectrum used in the ExMix simulations. A dust mode added ( $200 \mu\text{g m}^{-3}$ ) is plotted with a dashed line.

and dust concentration =  $600 \mu\text{g m}^{-3}$ . Figure 6b displays the plot of the total CCN number forming droplets with radii greater than  $3 \mu\text{m}$  versus the dust mass concentration, for various values of the dust solubility. We see that the number of CCN decreases when we add dust particles, except for  $\varepsilon = 1\%$ . Initially equal to  $304 \text{ cm}^{-3}$ , the CCN concentration decreases to  $211 \text{ cm}^{-3}$ , when dust concentration reaches  $600 \mu\text{g m}^{-3}$  and for a dust solubility  $\varepsilon$  of 20%. As previously, the decrease in CCN number forming droplets depends on the concentration and on the solubility of the mineral aerosol. Due to the assumption of an adiabatic parcel, all our computations give a LWC of  $0.375 \text{ g kg}^{-1}$  on the top of the stratocumulus layer. Thus it is quite normal that for a constant LWC, a decrease in droplet concentration leads to an increase in effective radius. However, it appears a contradiction in the fact to observe a decrease in CCN number when we add a significant number of dust particles.

[31] In order to explain this “paradox” and the different modifications of the droplet spectrum due to dust particles, we have plotted in Figure 7a the supersaturation curve of the parcel during the first moments of its ascent. The solid line represents the supersaturation of the parcel without the presence of dust. We observe a maximum value at the base of the cloud ( $0.37\%$  at  $t = 50 \text{ s}$ ), followed by a strong decrease which corresponds to the start of the condensation process of water vapor on the CCN, and a slight decrease up to values ranging from 0 to  $0.1\%$ . The dashed line in Figure 7a gives the supersaturation computed in the presence of dust with a concentration of  $400 \mu\text{g m}^{-3}$  and a solubility  $\varepsilon$  of 10%. The curve is similar to the previous one, except the maximum value at  $t = 50 \text{ s}$ , which reaches only  $0.27\%$  instead of  $0.37\%$ . This decrease in the maximum is probably due to the presence of dust particles, which can take a part of the available condensable water.

As large particles need less supersaturation to be activated than the small ones [Pruppacher and Klett, 1997], this fact plays an important role, because a decrease in supersaturation leads to a decrease also in the number of small activated particles. Figure 7b represents the scavenging ratio by nucleation of the aerosol distribution, with (dashed line) and without (solid line) addition of dust. We see a clear shift of the activation threshold toward the larger sizes when dust particles are added. Computations with the initial distribution show that some particles are activated for radii larger than  $0.06 \mu\text{m}$  and that 70% of the particles with radius equal to  $0.1 \mu\text{m}$  can form a droplet. When we add dust, no particles smaller than  $0.08 \mu\text{m}$  are activated, and less than 25% of the particles with radius equal to  $0.1 \mu\text{m}$  are scavenged, i.e., undergo the nucleation process. More generally, i.e., when dust particles are added to the other aerosols, the number of small particles (around  $0.1 \mu\text{m}$ ) serving as CCN significantly decreases. The radius values with which we are concerned correspond to the sulfate modes (especially mode 3, see Table 2). These particles are relatively numerous, and the shift of the activation threshold due to the presence of dust leads to a strong decrease in particles acting as CCN. This decrease is not numerically balanced by the dust particles. In fact, in our case, the addition of dust eliminates more small CCN particles than large particles are added. We see that there is no contradiction with the “Twomey effect,” which consists of a cloud albedo increase due to a decrease in the effective radius: This effect is obtained when, for instance, CCN are multiplied by 2 or 3, which is not our case here. We add a relatively small number of large particles with soluble material, so that the number of actual CCN decreases.

[32] Until here, we have not studied the role of the sulfate mass, which was kept constant with  $2.5 \mu\text{g m}^{-3}$ . Figure 8

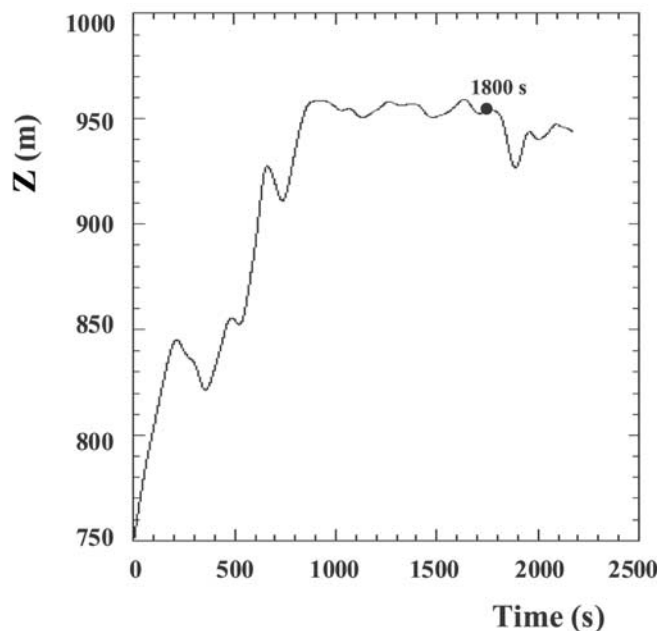


**Figure 4.** Air parcel vertical trajectory retained for the ExMix simulations. The “result point” (1800 s) is also represented.

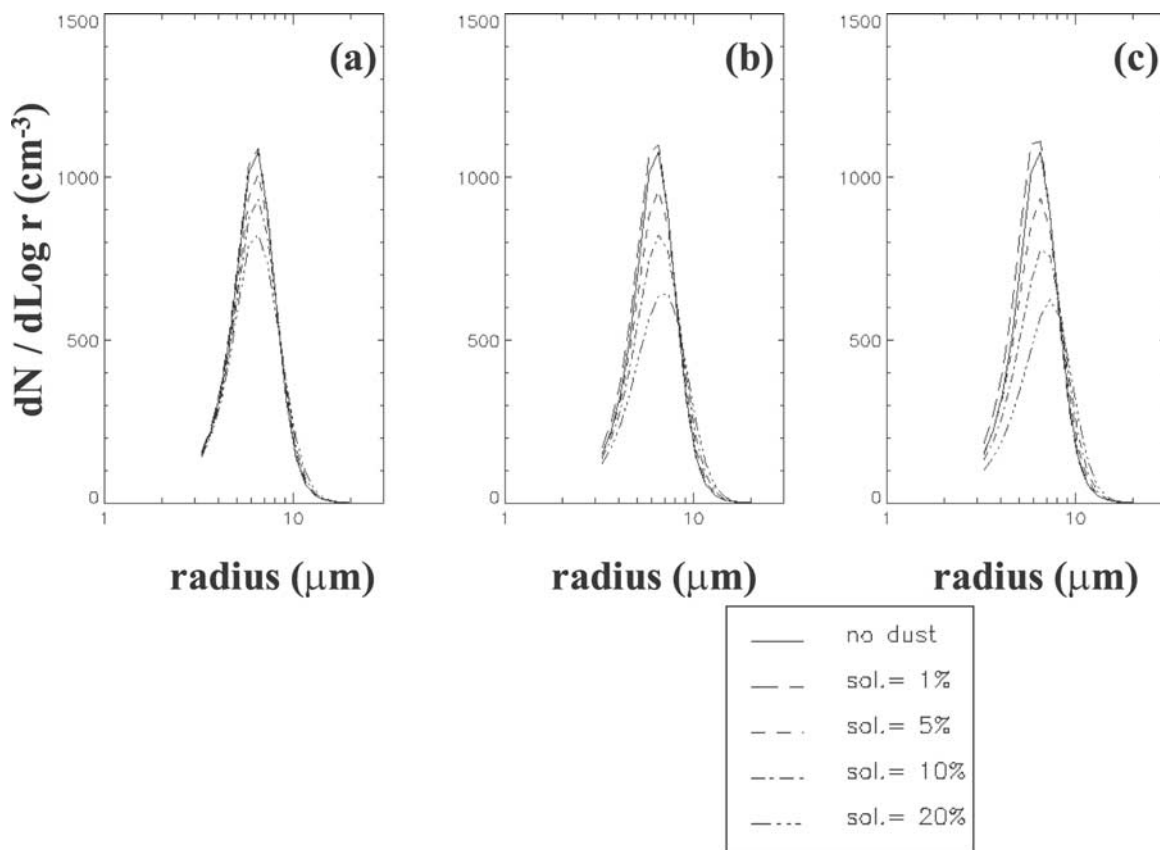


**Figure 5.** Droplet size distributions calculated with ExMix according to the aerosol properties described in the Table 2. Computations are made for (a)  $200 \mu\text{g m}^{-3}$ , (b)  $400 \mu\text{g m}^{-3}$  and (c)  $600 \mu\text{g m}^{-3}$  of dust added and for the different solubility values indicated. The reference droplet spectra calculated without dust particles are plotted as a solid line.

illustrates the influence of the total sulfate concentration (which is given by the modes 2 and 3) on the effective droplet radius. The variation of sulfate concentration is obtained by changing the total number of sulfate particles in modes 2 and 3 of the aerosol particle distribution given in Table 2. The results are computed for three dust concentrations and two values of dust solubility: 5% (Figure 8a) and 20% (Figure 8b). Here we assume that sulfate is present only as small particles (not associated with dust). As expected, there is a threshold of sulfate concentration above which the effective radius increases (and the CCN number decreases) when dust particles are added. Conversely, under the threshold, the addition of dust particles results in a decrease in the effective radius (and an increase in CCN number), which is a “Twomey effect” configuration. This threshold slightly depends on the dust solubility:  $1.5 \mu\text{g m}^{-3}$  for  $\epsilon = 5\%$  and  $1 \mu\text{g m}^{-3}$  for  $\epsilon = 20\%$ , whatever the dust concentration.

[33] We see that in pure marine condition, i.e., for low sulfate concentration, the presence of dust should lead to a decrease in the effective droplet radius. This result is very important, because it means that the influence of dust particles on the cloud properties depends also on the sulfate concentration and therefore on the anthropogenic pollution. We see that above a concentration of about  $3 \mu\text{g m}^{-3}$ , the dependence to the sulfate concentration becomes very weak. Anyway, we have seen (section 3.2.2) that sulfate

concentrations measured in winter west off the African coast are found near  $2.5 \mu\text{g m}^{-3}$  on average, because they are influenced by the African continental air masses. Note that such pollution levels are frequently exceeded over oceans: Simulations during the INDOEX campaign 1999 showed in agreement with experimental data that sulfate concentrations of more than  $2 \mu\text{g m}^{-3}$  are reached in the boundary layer over the Indian Ocean (G. Cautenet et al., Modeling the transport of aerosols during INDOEX 1999 and comparison with experimental data, 1, Carbonaceous aerosol distribution, submitted to *Journal of Geophysical Research*, 2002; F. Minvielle et al., Modeling the transport of aerosols during INDOEX 1999 and comparison with experimental data, 2, Continental aerosols and their optical depth, submitted to *Journal of Geophysical Research*, 2002). Thus, presuming that on average we are above the sulfate threshold (see Figure 8), the presence of dust particles leads to a decrease in CCN number and also to an increase in the effective droplet radius. As demonstrated above, these modifications modify the radiative properties of the cloud.

[34] The results of the ExMix model are now used as input in the radiative code described in the first section. The aim is to assess the effect of the modification of the droplet spectrum at the top of the stratocumulus layer due to the dust particles on the cloud optical properties. In Figure 9 is plotted the evolution of the system albedo  $\alpha$  against the dust

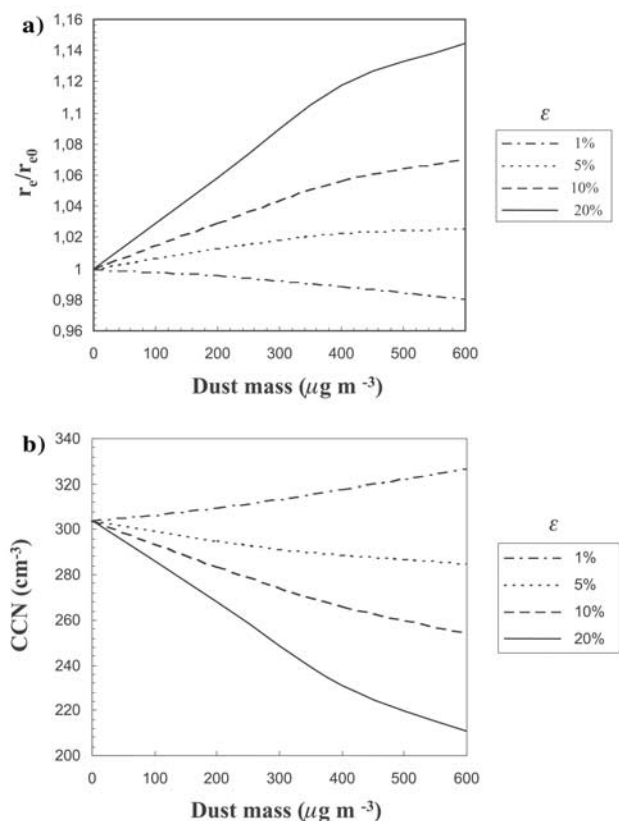


**Figure 6.** Effect of the dust mass added (a) on the droplet effective radius (normalized by the effective radius calculated without dust) and (b) on the CCN concentration. Computations with ExMix are made for the different solubility values indicated.

concentration. The results, for the four solubility values, are normalized by the albedo  $\alpha_0$  computed without dust. At  $t = 1800$  s, without dust, we find  $\alpha_0 = 0.42$ . We see that for a dust particles solubility of 1%, the increase in mineral aerosol concentration leads to a slight increase in albedo (about 1%). However, for higher values of solubility, the addition of dust particles leads to an albedo decrease. This decrease becomes more important when dust concentration and solubility increase. It is equal to 1.5% for a dust concentration of  $200 \mu\text{g m}^{-3}$  and a solubility of 10%. The maximum decrease in albedo is equal to 7%, found for the dust concentration of  $600 \mu\text{g m}^{-3}$  and a solubility of 20%.

### 3.2.4. Discussion

[35] To summarize, the addition of dust particles (with  $\epsilon > 1\%$ ) to the initial aerosol spectrum leads to a rise of the effective radius associated with a decrease in droplet number. These modifications of the droplet distribution should reduce the albedo of the considered cloud. We have seen that this decrease is strongly dependent on the dust solubility and on the dust concentration.

[36] Due to the complex processes that dust particles experience during their long-range transport, it appears

difficult to accurately assess their solubility values. Several microphysical or chemical mechanisms and many soluble species (sulfate, nitrate, sea salt...) are involved. However, according to computations and measurements detailed in section 3.1, it seems reasonable to assume a solubility value ranging between 5% and 15% far from the sources. The solubility seems also dependent on the particle size [Levin *et al.*, 1996], which, however, was not taken into account in our modeling. As mentioned in section 3.1, the solubility seems also to depend on the  $\text{SO}_2$  concentration, through formation of sulfate on the dust mode.

[37] According to the measurements of Chiapello *et al.* [1999], strong winter dust events may be translated by concentrations close to  $700 \mu\text{g m}^{-3}$  in the low layers over the ocean. Measurements (B. Chatenet, personal communication, 1999) at Sal Island in January 1995 reached about  $1000 \mu\text{g m}^{-3}$ . Following satellite data, Jankowiak and Tanré [1992] mentioned a dust outbreak with an aerosol optical thickness of about 2.8. Zhang [1994] gives values greater than  $800 \mu\text{g m}^{-3}$  to the east of Asia. In such conditions, and for a sulfate concentration high enough, an important decrease in cloud albedo may be expected. A simulation using ExMix with a dust concentration of  $800 \mu\text{g m}^{-3}$ , a dust solubility of 15% and a sulfate particles concentration of  $3 \mu\text{g m}^{-3}$ , reveal a decrease in albedo of the whole system close to 10%. Although this latter calculation involves extreme values, concentrations larger than  $200 \mu\text{g m}^{-3}$  are very common during dust outbreaks [Chiapello, 1996].

[38] So far, we have not really investigated the implications of the sulfate formation on the dust mode to the detriment of the accumulation mode, as mentioned and described in section 3.1. This phenomenon could enhance the increase of the dust effect on cloud albedo as estimated above. Indeed, the mechanism of transfer of sulfate mass toward the large particles should lead to a deficit in small particles (very active as CCN). Figure 10 shows the influence of the decrease (in percent) of the sulfate concentration in the accumulation mode on the cloud albedo  $\alpha$ .  $\alpha_0$  is the albedo calculated without dust and with the initial sulfate concentration, i.e.,  $2.5 \mu\text{g m}^{-3}$ . Prior to all, we must keep in mind that the solubility of dust particles is an experimental fact and ranges between 5% and 15%. This property is not only dependent on the sulfate transfer process, but is also due to the whole history of the dust along its long travel: dissolution process, capture of various species, etc. All these phenomena have not been modeled here. For this reason, the calculations presented here are made with constant values of  $\epsilon$ . In the solid line, we have the effect of  $200 \mu\text{g m}^{-3}$  of dust with a solubility equal to 10%, and in dashed line  $600 \mu\text{g m}^{-3}$  of dust with  $\epsilon = 20\%$ . The general trend is an accentuation of the albedo decrease when a particulate sulfate reduction is added to the “pure” dust effect. This effect was expected, because a reduction of small sulfate particles means once again a decrease in CCN number and an increase of the droplet effective radius. Note that the effect of sulfate reduction (accumulation mode) is more efficient for the  $200 \mu\text{g m}^{-3}$  ( $\epsilon = 10\%$ ) concentration than for the  $600 \mu\text{g m}^{-3}$  ( $\epsilon = 20\%$ ) one. It may be explained by the fact that  $600 \mu\text{g m}^{-3}$  of dust particles have a very strong effect on the initial aerosol distribution. By the shift of the nucleation threshold (see Figure 7b), a large part of

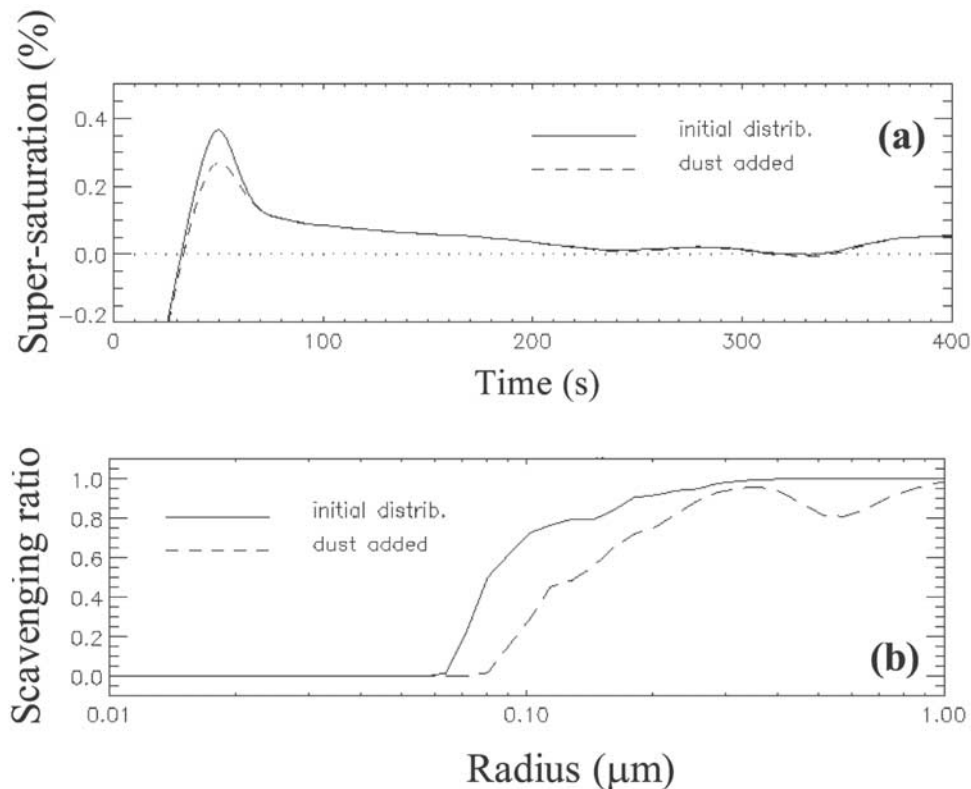


**Figure 7.** (a) Supersaturation (in percent) of the air parcel versus the time and (b) scavenging ratio by nucleation of the aerosol distribution, with (dashed line) and without (solid line) addition of  $400 \mu\text{g m}^{-3}$  of dust particles ( $\varepsilon = 10\%$ ).

sulfate particles do not act as CCN anymore. Therefore a reduction of their number has a lower impact on the droplet distribution and on the cloud albedo. However, for  $200 \mu\text{g m}^{-3}$  (typical value during dust events), the effect of this decrease of sulfate mass is very significant. Where the decrease of the system albedo is equal to 1.5% due to the “pure” effect of dust particles, the reduction of 50% of the sulfate mass in the accumulation mode leads to a total decrease of about 5%. For the same sulfate fraction reduction and  $600 \mu\text{g m}^{-3}$  of dust, the albedo decrease takes values from about 7% to 8%. According to literature mentioned in the section 3.1, 50% to 80% of the sulfate mass may be associated with the dust mode. Following our calculations, that should induce a total decrease in albedo of the system ranging between 5% and 10% for  $200 \mu\text{g m}^{-3}$  of dust, and between 7% and 9% for  $600 \mu\text{g m}^{-3}$ . Moreover, the few large droplets formed on dust particles may lead to the coalescence process [Feingold *et al.*, 1999; Wurzler *et al.*, 2000], a microphysical mechanism not considered in our model. That could cause the formation of larger droplets and a larger decrease in the cloud albedo, although the initial droplet distribution (without dust added) does not present many large droplets.

[39] During dust events, the influence of dust particles on stratocumulus cloud properties is therefore obvious and may have a significant regional radiative impact. These results are also very important concerning the assessment, using large-scale models, of the global indirect effect due to sulfate. To consider the mass of sulfate as a whole, and not to take into account the significant part associated with the large-particle mode in the regions where dust concentration is high, could

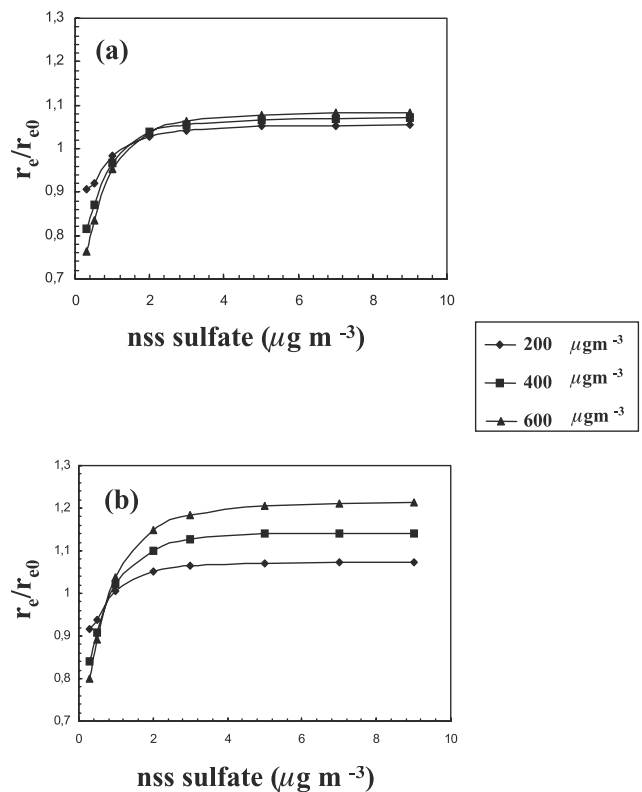


**Figure 8.** Effect of the nss sulfate concentration on the modification of the effective radius by the dust particles, for (a)  $\varepsilon = 5\%$  and (b)  $\varepsilon = 20\%$ . The concentrations of dust added are indicated.

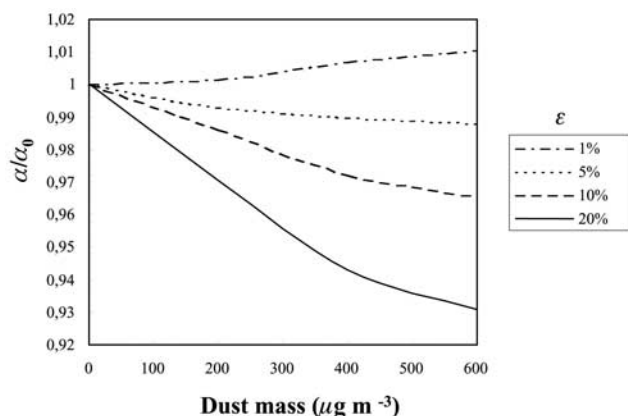


**Figure 9.** Normalized albedo of the cloud system versus the concentration of dust added. Solubility values of dust are mentioned (in percent).

induce a significant overestimation (which may reach 10%) of the albedo of the marine lower cloud.

## 4. Discussion About Direct and Indirect Effect

### 4.1. Overview

[40] The radiative simulations of section 2 show that in summer, the average dust concentration found over the cloud cover may explain the observations, i.e., the apparent albedo decrease observed by satellite.

[41] In winter, dust particles travel in major part at the same level as the cloud cover, in the TWL, causing a decrease in the apparent cloud albedo up to 10%. In section 3 of the present paper we showed that a high concentration of dust may strongly affect the stratiform clouds albedo in winter. However, these dust plumes are not a permanent feature over the studied areas. Satellite observations detailed in the part 1 of this study revealed an occurrence of “dusty days” (high dust concentration) ranging between 30% and 60% over the areas where the albedo decrease is observed. According to measurements of Si and Al concentration at Sal Island during winter [Chiapello *et al.*, 1996], the dust concentration ranges between  $70 \mu\text{g m}^{-3}$  and  $100 \mu\text{g m}^{-3}$  on average (calculated over 4 years), because of the count of the “clear days” (without dust) in the average. Husar *et al.* [1997], who averaged AVHRR data over three winter months, found a dust optical thickness of about 0.5 to the west of the African coast. Therefore, on average, the mean radiative effect of dust on the cloud albedo is certainly lower. Inversely, the coalescence processes mentioned in the previous section could enhance this radiative effect. According to our model results, we suggest an average value for the system albedo decrease ranging between 3% and 10%. This value could explain in a large part the “deficit” in albedo (between 10% and 15%) observed by satellite during the winter season.

[42] In addition, a simple complementary explanation for this albedo decrease could be the presence of carbonaceous particles from biomass burning over the studied area. We discuss this possibility in the following section.

### 4.2. Modeling of Transport and Radiative Effect of the Carbonaceous Particles

[43] It is well known that in January, large areas in tropical Africa (Northern Hemisphere) undergo the phenomenon of vegetation fires. According to Barbosa *et al.* [1999], the annual burned biomass from vegetation fires in Africa ranges between about 700 and 2200 Mt. These fires concern especially the tropical savanna vegetation. About 1600 Mt of African savanna burn every year [Hao and Liu, 1994]. During the winter months, a large band of savanna is concerned between about  $5^{\circ}\text{N}$  and  $15^{\circ}\text{N}$  in Africa, from the west coast up to about  $30^{\circ}\text{E}$  [Lioussse *et al.*, 1997; Barbosa *et al.*, 1999]. These fires produce mainly submicronic black carbon particles (BC) and particulate organic matter (POM) [Lioussse *et al.*, 1996a]. These emissions may be transported by the wind over the Atlantic Ocean, either westward or southward (Gulf of Guinea). According to earlier large-scale simulations of Lioussse *et al.* [1996b], a significant amount of carbonaceous particles (CP) is found off western and southern African coasts in January, particularly below  $10^{\circ}\text{N}$ . Measurements in November [Ketsederis *et al.*, 1976; Andreae, 1983] give values of POM ranging between  $0.33$  and  $1.60 \mu\text{g m}^{-3}$  at sea surface near  $15^{\circ}\text{N}$  and  $27^{\circ}\text{W}$  (west of the Cape Verde Islands). A plume of carbonaceous particles transported over the oceanic stratocumulus field could have an impact on the albedo of the system. The question is to know more accurately the geographic position and the altitude of these plumes over the Atlantic Ocean, and to assess their particle concentration, so as to be able to estimate their optical impact.

[44] In order to answer these different questions, we have simulated the transport of CP, represented by the black carbon (BC), during January 1993. We use the Regional

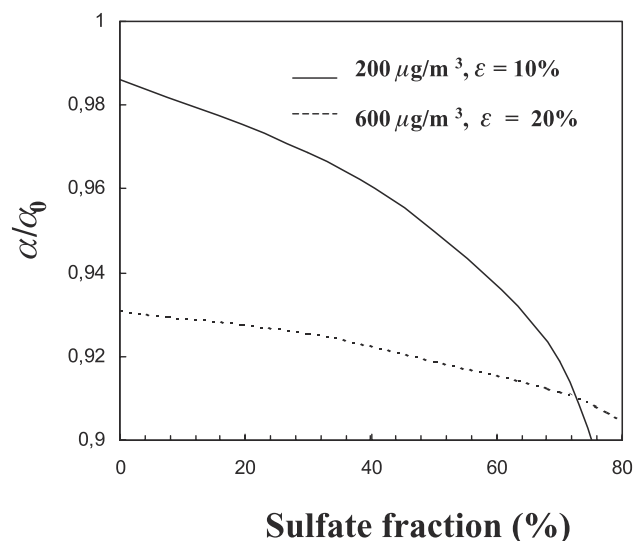


**Figure 10.** Normalized albedo of the cloud system versus the fraction of sulfate mass (in percent) transferred to the large mode to the detriment of the accumulation mode.  $\alpha_0$  is the albedo calculated without dust and with the initial sulfate concentration, i.e.,  $2.5 \mu\text{g m}^{-3}$ .

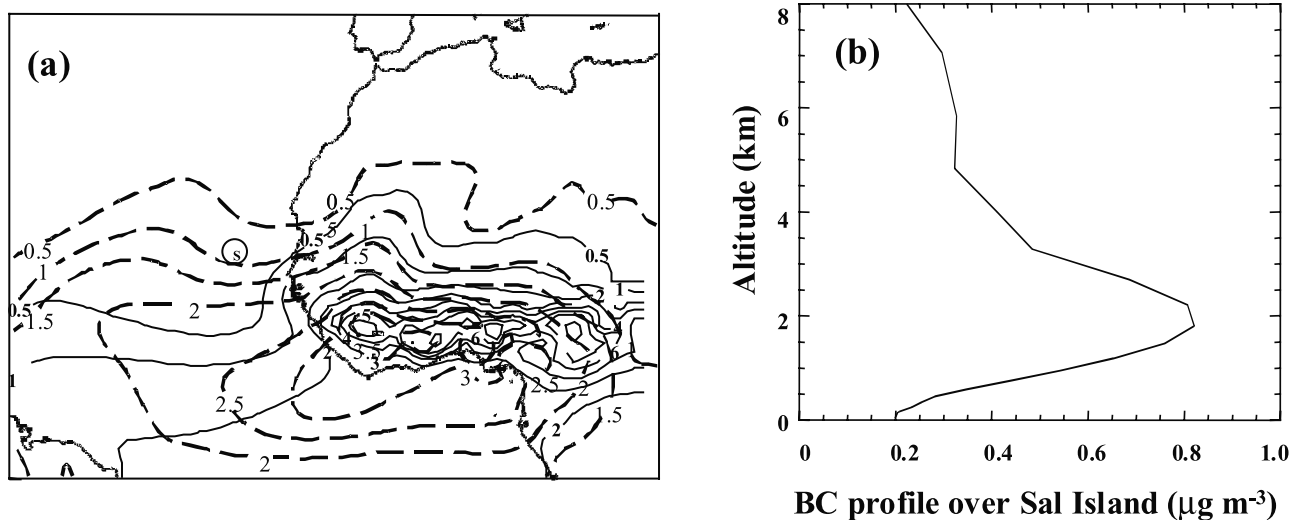


**Figure 11.** (a) Averaged model values (third decade of January 1993) of BC concentration ( $\mu\text{g m}^{-3}$ ) at two levels above surface: 100 m (solid lines, small bold labels) and 2200 m (dashed lines, fine larger labels). Letter S in a circle: Sal Island and Cape Verde archipelago. (b) Vertical modeled BC profile over Sal Island (averaged over the third decade of January 1993).

Atmospheric Modeling System (RAMS; *Pielke et al.* [1992]) of the Colorado State University. We use the non-hydrostatic version “3b.” It has recently been used to address problems connected with transport of anthropogenic or natural contaminant in Africa, including desert dust transport toward Mediterranean [*Cautenet et al.*, 2000] or biomass burning over central Africa [*Cautenet et al.*, 1999; *Poulet*, 2000]. The modeled domain covers an area that ranges from  $45^{\circ}\text{W}$  to  $25^{\circ}\text{E}$  and from  $5^{\circ}\text{S}$  to  $34^{\circ}\text{N}$ . We use a single grid with a horizontal grid step of 100 km. The topography is derived from the NOAA database. The vertical grid is subdivided into 30 layers, increasing with height. The first 10 levels are located within the lowest 1500 m, which generally corresponds to the fully developed tropical boundary layer. The ECMWF analyzed fields are used to initialize the model runs and also to control the atmospheric parameters at synoptic scale. In our simulations, we have used a BC source which we derived from the analysis of the Global Fire Product GFP (1993), using the IGBP-Data and the 1 km Advanced Very High Resolution Radiometer (AVHRR) Global Land Project data set [*Grégoire et al.*, 1999]. Starting from the fire areas detected by satellite, the BC vertical fluxes are assessed every day following a mass emission formulation derived from *Crutzen et al.* [1979]. Finally, we mapped the daily BC source in a longitude-latitude grid. As the RAMS model uses a polar stereographic system of coordinates, tangent to the Earth surface in a point that is called the pole, we have transformed the source data into this special coordinate system prior to incorporating them in the model. A time modulation is introduced in the emission scheme, according to the agricultural practices as observed by the authors; that is, the major part of the emission takes place during daytime. The injection of tracer BC into the atmosphere is modeled as follows: At each time step, a given amount of BC, estimated from the source intensity, is homogeneously diluted into the first 100 m above the surface. This amount

is transformed into a mixing ratio and added to the tracer, and consequently advected and diffused by RAMS in time and space. Moreover, at each time step, the deposition scheme modifies the concentrations near surface: A turbulent dry deposition velocity of  $0.2 \text{ cm s}^{-1}$  is assumed in the first atmospheric layer. We do not include any wet scavenging. We obtain BC concentrations at any time and grid point. For more information about using the RAMS model coupled with pollutant sources, see, e.g., *Cautenet et al.* [1999, 2000].

[45] The detailed results of this modeling are to be published in a paper in preparation. Here we merely try to illustrate a possible interaction between CP and cloud leading to a decay in the apparent albedo. The simulations start with a “clean” atmosphere without carbonaceous aerosol particles. A quasi-stationary regime is quickly reached after a few days. Figure 11 represents the BC concentration averaged over the third decade of January 1993. Over the Ocean, we note (Figure 11a) that concentrations near surface are weaker than at 2 km. This is illustrated by the vertical profile in Figure 11b. As the thicker part of the BC plume is found at 2 km (i.e., above the cloud cover), a radiative direct effect may be expected. In order to assess approximately this radiative effect, we have computed the average optical thickness at 550 nm for a zonally averaged ( $10^{\circ}$  in width) meridional strip centered on Cape Verde archipelago. We first compute the columnar load, and then we multiply it by the BC absorption efficiency (thus neglecting the scattering effect of BC and OC). This absorption efficiency is taken equal to  $7 \text{ m}^2 \text{ g}^{-1}$ , according to *Lioussé et al.* [1996b]. The results are displayed in Figure 12. According to this curve and Figure 11b, we find a contribution of the BC to the optical thickness ranging between 0.02 and 0.06 above a typical stratocumulus cloud. The subsequent decay in albedo ranges between 1.5% and 4%. Added to the dust particle effect, that could lead to a total decrease in albedo between 5% and

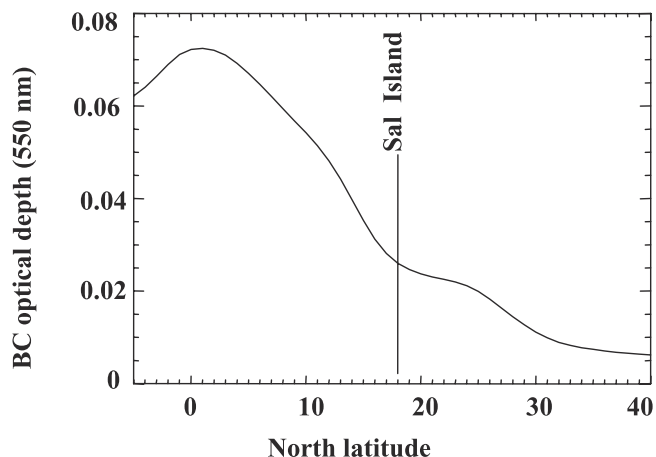


**Figure 12.** Zonal average ( $\pm 5^\circ$  around the Sal Island meridian) of the 550 nm BC optical thickness, averaged over the third decade of January 1993.

15%, which is in accordance with the values derived from satellite measurements performed in winter.

#### 4.3. Results for the Radiative Forcing

[46] In this section, we will give a first (and rough) assessment of the radiative impact of the aerosol particles in the shortwave spectrum.

##### 4.3.1. Winter Case, No BC Effects

[47] Ignoring the presence of the BC effect, we calculate the solar net radiative fluxes at the surface for a cloud albedo decrease due to the increase of the effective radius, as discussed in the section 3.2. We simulate the radiative forcing when  $r_e$  evolves from the “basic” value of  $7.4 \mu\text{m}$  to a typical, microphysically increased value of  $8.6 \mu\text{m}$ . We have seen that this is likely to occur during the wintertime, when dust microphysically interacts with the cloud. We consider again the typical stratocumulus that we have already used above in section 2. Under such conditions, we have computed the surface radiative forcing. The forcing is defined as the difference between the average surface net solar radiation computed with both values of the effective radius, on January 15 at  $15^\circ\text{N}$ . The EC3 model is run for a complete diurnal cycle, and the results are averaged over the 24-hour period. We find  $+10 \text{ Wm}^{-2}$ : This forcing is positive when the effective radius increases. According to our hypotheses, this may be attributed to microphysical interactions between dust and clouds only, without any BC effect.

##### 4.3.2. Winter Case, Including BC Effects

[48] Now we keep the same hypotheses as above, but we assume a 2 km thick BC layer above the cloud, with a shortwave optical depth of 0.05, a typical high value as stated in section 4.2. The surface radiative forcing (for January 15 and  $15^\circ\text{N}$ ) is now reduced and is equal to only  $+6 \text{ Wm}^{-2}$ . On the other hand, the radiative forcing of the BC layer is  $+9 \text{ Wm}^{-2}$ . A broad assessment of the radiative heating of the BC layer is about  $+0.4 \text{ K d}^{-1}$ .

##### 4.3.3. Summer Case

[49] Finally, we assume that the stratocumulus is not modified, i.e.,  $r_e = 7.4 \mu\text{m}$  and a 2 km thick dust layer above the cloud. The shortwave dust optical thickness is

taken equal to 0.5, a typical value as discussed in section 2. Now, the surface budget decreases significantly: The surface forcing is  $-13 \text{ Wm}^{-2}$ . This decrease is compensated by a strong increase in the dust layer radiative forcing, which reaches  $+37 \text{ Wm}^{-2}$ . The radiative heating of the dust layer reaches about  $+1.6 \text{ K d}^{-1}$ .

[50] We may conclude that dust always has a positive shortwave impact on the atmospheric column (from surface to top of atmosphere) when clouds are present. However, according to the position of the aerosol layer, the location of the heating/cooling zones may be modulated in position and sign. It may be noted that previous works [see, e.g., Cautenet *et al.*, 1992; Jankowiak, 1992] show that dust alone (no clouds) has a negative impact on the global column budget. In our study, however, dust and clouds are present in the same column. Furthermore, our results suggest that dust (and other aerosols, BC in our case) could modify the negative shortwave forcing of clouds in adding small quantities of heat to the global surface-atmosphere column.

## 5. Conclusion

[51] According to the first part of this paper, the stratiform cloud cover of the West African coast presents a slight but nonnegligible anomaly in visible reflectivity. This anomaly seems to coincide with the presence of mineral dust plumes originating from Saharan or Sahelian areas. In order to assess the radiative effect of a dust plume in the presence of a stratiform cloud and to explain the satellite observations, we have first presented radiative simulations using the “EC3” version of the ECMWF radiative code. It appears that the presence of a dust layer over the cloud cover (i.e., summer configuration) leads to a significant decrease in albedo of the ocean-cloud-atmosphere system, due to the slight but nonnegligible absorptivity of the mineral aerosol. We considered a 150 m thick stratocumulus with a droplet effective radius  $r_e = 7 \mu\text{m}$  and a dust plume above the cloud layer. The albedo decreases by almost 30% for a visible optical thickness  $\tau = 1$  of the dust plume. For  $\tau$  equal to 0.5, which is a commonly observed value during the summer months between  $15^\circ\text{N}$  and  $25^\circ\text{N}$ , the corresponding simulated albedo decrease is about 15%. Therefore this direct radiative effect by superposition of clouds and aerosol particles could alone explain the albedo decrease of the system as observed in summer by satellite.

[52] On the other hand, our radiative simulations are not able to justify the strong albedo decrease observed in winter: With dust lying in the TWL, we only get a variation of a few percent of the system albedo, independently of the optical thickness of the dust plume. Note that all these results are not dependent on the LWC of the stratocumulus top, provided that it is greater than  $0.2 \text{ g kg}^{-1}$ . We therefore have investigated another way for the winter configuration: the microphysical interactions between dust particles and water clouds. Using the microphysical model ExMix, our simulations show that a large concentration of dust particles would strongly affect the droplet distribution of a stratiform cloud. When the soluble fraction of dust is high enough (say, for  $\varepsilon > 3\%$ ), the presence of large mineral particles induces (1) a decrease of the supersaturation value, (2) a subsequent shift in the activation threshold toward the larger

nuclei and (3) a decrease in the CCN number, provided that the sulfate concentration is greater than  $1 \mu\text{g m}^{-3}$  in our simulations. As the LWC of the adiabatic cloud parcel remains constant, the decrease in CCN number is associated with an increase of the effective radius of the droplets at the cloud top, and a decrease of the cloud albedo.

[53] Results from the literature show that dust particles, which are initially hydrophobic ( $\epsilon \approx 0$ ), may reach solubility values ranging between 5% and 15%. Different studies mention that dust particles are generally associated with very soluble chemical species (sulfates, nitrates...), after in-cloud processing or chemical reactions (either gaseous or aqueous) on their surface during their long-range transport. Measurements reveal the presence of nonnegligible sulfate concentration ( $>2 \mu\text{g m}^{-3}$ ) over the studied area, i.e., the tropical northeastern Atlantic Ocean. We have included these different parameters in our simulations. We show that the effect of a high dust load associated with a significant sulfate concentration leads to a decrease in the albedo of about 10%. Locally, a strong dust outbreak (say,  $>500 \mu\text{g m}^{-3}$ ) may therefore strikingly affect the albedo of the clouds. On average, however, dust concentrations are lower, due to the sporadic nature of the dust outbreaks, and thus lead to a lower effect. Nevertheless, due to in-cloud processes and surface chemical reactions involving dust particles, a transfer process of sulfate from the accumulation mode to the dust mode occurs, associated with a decrease of the efficient CCN number, and also may contribute to the cloud albedo decrease. We can reasonably assess an apparent average albedo decrease ranging between 3% and 10% in winter, i.e., below the observed values ranging from 10% to 15%.

[54] The biomass burning in the northern intertropical part of Africa in winter (dry season) may be a complementary physical explanation to the apparent albedo decrease. According to simulations using the RAMS model, a fraction of the carbonaceous particles emitted by savanna fires, i.e., BC (and also organic carbonaceous particles, but much less absorbing than BC in the visible), may travel westward up to the tropical Atlantic Ocean. Following the dynamical climatology of these region, simulations (performed in January 1993) reveal that a large part of these particles is found above the TWL, that is to say, above the cloud cover, over our study area. As the carbonaceous aerosols (and especially the BC) are strong light absorbing particles, they also can reduce the albedo of the system in winter (as does a dust plume in the summer configuration). For the BC concentrations computed with RAMS, the associated albedo decrease ranges between 1.5 and 4%. We therefore may conclude that in winter, the complex microphysical effects of dust and the presence of absorbing carbonaceous particles at altitude could explain the decrease of apparent cloud albedo observed by satellite.

[55] In both cases (summer or winter configurations), our computations are in rather good agreement with the satellite observations. Through direct or indirect effects, they put forward the role and the positive radiative forcing induced by particles, in particular mineral dust in the presence of clouds over the tropical northeastern Atlantic Ocean.

[56] Finally, we presented a tentative estimate of the radiative impact of aerosols over the area. The average short-wave effect is dependent on the relative position of

clouds and dust layer. The average forcing is positive (about  $+10 \text{ Wm}^{-2}$ ) near the surface in the winter case without BC and positive in the surface layer and in the BC layer in winter when BC is present ( $+6 \text{ Wm}^{-2}$  and  $+9 \text{ Wm}^{-2}$ , respectively). In summer, the forcing is negative ( $-13 \text{ Wm}^{-2}$ ) in the surface layer and positive ( $+37 \text{ Wm}^{-2}$ ) in the overlying dust layer. These results suggest that dust is likely to modify the radiative shortwave budget of the atmospheric column in the presence of clouds.

[57] **Acknowledgments.** Our work is supported by funding of the French Centre National de la Recherche Scientifique (CNRS), in particular by the Programme National de Chimie Atmosphérique. The authors wish to thank W. Wobrock (LaMP) for his help concerning the ExMix model, P. Laj (LaMP) for the initial aerosol distribution and the ACE-2 HILLCLOUD data, and D. Poulet for his assistance in biomass burning assessments. They thank also the computer team of the LaMP: R. Pejoux, A.M. Lanquette and F. Besserve. This work makes use of the RAMS model, which was developed under the support of the National Science Foundation (NSF) and the Army Research Office (ARO). We have used the computer resources of the CINES (Centre Informatique national de l'enseignement supérieur, projet amp2106).

## References

- Ackerman, A. S., O. B. Toon, and P. V. Hobbs, Numerical modeling of ship tracks produced by injections of cloud condensation nuclei into marine stratiform cloud, *J. Geophys. Res.*, *100*, 7121–7133, 1995.
- Alfaro, S., A. Gaudichet, L. Gomes, and M. Maille, Mineral aerosol production by wind erosion: Aerosol particle sizes and binding energies, *Geophys. Res. Lett.*, *25*, 991–994, 1998.
- Andreae, M. O., Soot carbon and excess potassium: Long-range transport of derived aerosols, *Science*, *220*, 1148–1151, 1983.
- Andreae, M. O., R. J. Charlson, F. Bruynseels, H. Storms, R. van Grieken, and W. Maenhout, Internal mixture of sea salt, silicates, and excess sulfate in marine aerosols, *Science*, *232*, 1620–1623, 1986.
- Barbosa, P. M., D. Stroppiana, J.-M. Gregoire, and J. M. C. Pereira, An assessment of vegetation fire in Africa (1981–1991): Burned areas, burned biomass, and atmospheric emissions, *Global Biogeochem. Cycles*, *13*(4), 933–950, 1999.
- Bower, K. N., et al., ACE-2 HILLCLOUD: An overview of the ACE-2 ground-based cloud experiment, *Tellus, Ser. B*, *52*, 750–778, 2000.
- Brenguier, J. L., P. Y. Chuang, Y. Fouquart, D. W. Johnson, F. Parol, H. Pawlowska, J. Pelon, L. Schüller, F. Schröder, and J. Snider, An overview of the ACE-2 CLOUDCOLUMN experiment, *Tellus, Ser. B*, *52*, 815–827, 2000.
- Cautenet, G., M. Legrand, S. Cautenet, B. Bonnel, and G. Brogniez, Thermal impact of Saharan dust over land, part I, Simulation, *J. Appl. Meteorol.*, *31*, 166–180, 1992.
- Cautenet, G., F. Guillard, B. Marticorena, G. Bergametti, F. Dulac, and J. Edy, Modeling of a Saharan dust event, *Meteorol. Z.*, *9*, 221–230, 2000.
- Cautenet, S., D. Poulet, C. Delon, R. Delmas, J.-M. Grégoire, J. M. Pereira, S. Cherchali, O. Amram, and G. Flouzat, Simulation of carbon monoxide redistribution over central Africa during biomass burning events (EXPRESSO experiment), *J. Geophys. Res.*, *104*, 30,641–30,658, 1999.
- Charlson, T. J., J. E. Lovelock, M. O. Andreae, and S. G. Warren, Oceanic phytoplankton, atmospheric sulphur, cloud albedo, and climate, *Nature*, *326*, 655–661, 1987.
- Chiapello, I., Les aérosols atmosphériques au-dessus de l'Atlantique Nord tropical: Approche physico-chimique et météorologique, Evaluation de la contribution des différentes espèces à l'épaisseur optique en aérosol, thèse de doct., l'Univ. Paris 7, 1996.
- Chiapello, I., G. Bergametti, L. Gomes, B. Chatenet, F. Dulac, J. Pimenta, and E. Santos Soares, An additional low layer transport of Sahelian and Saharan dust over the north eastern tropical Atlantic, *Geophys. Res. Lett.*, *22*, 3191–3194, 1995.
- Chiapello, I., G. Bergametti, B. Chatenet, P. Bousquet, F. Dulac, and E. Santos Soares, Origins of African dust transported over the northeastern tropical Atlantic, *J. Geophys. Res.*, *102*, 13,701–13,709, 1997.
- Chiapello, I., G. Bergametti, B. Chatenet, F. Dulac, I. Jankowiak, C. Lioussé, and E. Santos Soares, Contribution of the different aerosol species to the aerosol mass load and optical depth over the northeastern tropical Atlantic, *J. Geophys. Res.*, *104*, 4025–4035, 1999.
- Chomette, O., Modélisation et analyse méso-échelle du cycle de l'aérosol désertique: Aspects radiatifs et dynamiques, thèse de doct., Univ. de Lille 1, Lille, France, 1999.

- Clark, T. L., A small scale dynamic model within a two dimensional dynamic framework, *J. Comput. Phys.*, 24, 2393–2405, 1977.
- Clark, T., Numerical simulation of 3-D cloud model, *J. Atmos. Sci.*, 36, 2191–2215, 1979.
- Crutzen, P. J., L. E. Heidt, J. P. Krasnec, W. H. Pollock, and W. Seiler, Biomass burning as a source of atmospheric gases, CO, H<sub>2</sub>, N<sub>2</sub>O, NO, CH<sub>3</sub>CL, and COS, *Nature*, 282, 253–256, 1979.
- d'Almeida, G. A., P. Koepke, and E. P. Shettle, *Atmospheric Aerosols, Global Climatology and Radiative Characteristics*, 561 pp., A. Deepak, Hampton, Va., 1991.
- Dentener, F. J., G. R. Carmichael, Y. Zhang, J. Lelieveld, and P. J. Crutzen, Role of mineral aerosol as a reactive surface in the global troposphere, *J. Geophys. Res.*, 101, 22,869–22,889, 1996.
- Desboeufs, K. V., R. Losno, F. Vimeux, and S. Cholbi, The pH-dependent dissolution of wind-transported Saharan dust, *J. Geophys. Res.*, 104, 21,287–21,299, 1999.
- Eichel, C., M. Krämer, L. Schütz, and S. Wurzler, The water-soluble fraction of atmospheric aerosol particles and its influence on clouds microphysics, *J. Geophys. Res.*, 101, 29,499–29,510, 1996.
- Feingold, G., W. R. Cotton, S. M. Kreidenweiss, and J. T. Davis, The impact of giant cloud condensation nuclei on drizzle formation in stratocumulus: Implications for cloud radiative properties, *J. Atmos. Sci.*, 24, 4100–4117, 1999.
- Fouquart, Y., and B. Bonnel, Computation of solar heating of the Earth's atmosphere: A new parameterization, *Contrib. Atmos. Phys.*, 53, 35–52, 1980.
- Fouquart, Y., B. Bonnel, and V. Ramaswamy, Intercomparing shortwave radiation codes for climate studies, *J. Geophys. Res.*, 96, 8955–8968, 1991.
- Frouin, R., C. Gauthier, and J. J. Morcrette, Downward longwave irradiance at the ocean surface from satellite data: Methodology and in situ validation, *J. Geophys. Res.*, 93, 597–619, 1986.
- Gérémy, G., W. Wobrock, A. I. Flossmann, A. Schwarzenböck, and S. Mertes, A modelling study on the activation of small Aitken-mode aerosol particles during CIME 97, *Tellus, Ser. B*, 52, 959–979, 2000.
- Grégoire, J.-M., S. Pinnock, E. Dwyer, and E. Janodet, Satellite monitoring of vegetation fires for espresso: Outline of activity and relative importance of the study area in the global picture of biomass burning, *J. Geophys. Res.*, 104, 30,691–30,699, 1999.
- Guelle, W., Comparaison des simulations globales de <sup>210</sup>Pb et d'aérosols sahariens aux observations de surface et satellitaires, thèse de doct., l'Univ. de Paris 7, 1998.
- Hao, W. M., and M. H. Liu, Spatial and temporal distribution of tropical biomass burning, *Global Biogeochem. Cycles*, 8(4), 495–503, 1994.
- Hindman, E. E., and R. J. Bodowski, A marine stratus layer modified by nuclei from a ship plume, *J. Appl. Meteorol.*, 35, 1596–1600, 1996.
- Horai, S., I. Minari, and Y. Migita, Aerosols composition in Kagoshima, *Annu. Rep. 9*, Kagoshima Prefectural Inst., Kagoshima, Japan, 1993.
- Husar, R. B., J. M. Prospero, and L. L. Stowe, Characterization of tropospheric aerosols over the oceans with the NOAA advanced very high resolution radiometer optical thickness operational product, *J. Geophys. Res.*, 102, 16,889–16,909, 1997.
- Jankowiak, I., Surveillance des aérosols désertiques à partir de l'imagerie Meteosat et estimation de leur impact radiatif, thèse de doct., Univ. de Lille 1, Lille, France, 1992.
- Jankowiak, I., and D. Tanré, Satellite climatology of Saharan dust outbreaks, *J. Clim.*, 5, 646–656, 1992.
- Ketsederis, G., J. Hahn, R. Jaenicke, and C. Junge, The organic constituents of atmospheric particulate matter, *Atmos. Environ.*, 10, 603–610, 1976.
- Kim, Y., and R. D. Cess, Effect of anthropogenic sulfate aerosols on low-level cloud albedo over oceans, *J. Geophys. Res.*, 98, 14,883–14,885, 1993.
- Levin, Z., E. Ganor, and V. Gladstein, The effects of desert particles coated with sulfate on rain formation in the eastern Mediterranean, *J. Appl. Meteorol.*, 35, 1511–1523, 1996.
- Liousse, C., J. E. Penner, J. J. Walton, H. Eddleman, C. Chuang, and H. Cachier, Modeling biomass burning aerosols, in *Biomass Burning and Global Change*, vol. 1, edited by J. S. Levine, pp. 492–508, MIT Press, Cambridge, Mass., 1996a.
- Liousse, C., J. E. Penner, C. Chuang, J. J. Walton, and H. Eddleman, A global three-dimensional study of carbonaceous aerosols, *J. Geophys. Res.*, 101, 19,411–19,432, 1996b.
- Liousse, C., F. Dulac, H. Cachier, and D. Tanré, Remote sensing of carbonaceous aerosol production by African savanna biomass burning, *J. Geophys. Res.*, 102, 5895–5911, 1997.
- Mamane, T., E. Ganor, and A. Donagi, Aerosol composition of urban and desert origin in the Eastern Mediterranean, *Water Air Soil Pollut.*, 14, 29–43, 1980.
- Martin, G. M., D. W. Johnson, and A. Spice, The measurement and parameterization of effective radius of droplets in warm stratocumulus clouds, *J. Atmos. Sci.*, 51, 1823–1842, 1993.
- McClatchey, R. A., W. S. Benedict, S. A. Clough, D. E. Burch, R. F. Calfee, K. Fox, L. S. Rothman, and J. S. Garing, AFCRL atmospheric absorption line parameters compilation, *AFCRL-TR-73-0096*, Environ. Res. Pap. 434, 78 pp., Bedford, Mass., 1973.
- Morcrette, J. J., Description of the radiation scheme in the ECMWF model, *Tech. Memo. 165*, 26 pp., Res. Dep., Eur. Cent. for Medium-Range Weather Forecasts, Reading, England, 1989.
- Morcrette, J. J., and Y. Fouquart, The overlapping of cloud layers in short-wave radiation parameterizations, *J. Atmos. Sci.*, 43, 321–328, 1986.
- Morcrette, J. J., L. Smith, and Y. Fouquart, Pressure and temperature dependence of the absorption in longwave radiation parameterizations, *Contrib. Atmos. Phys.*, 59, 455–469, 1986.
- Nishikawa, M., and S. Kanomari, Chemical composition of Kosa aerosol (yellow sand dust) collected in Japan, *Anal. Sci.*, 7, 1127–1130, 1991.
- Parungo, F., Y. Kim, C.-J. Zhu, J. Harris, R. Schnell, X. S. Li, D.-Z. Yang, M.-Y. Zhou, Z. Chen, and K. Park, Asian dust storms and their effects on radiation and climate, *STC Rep. 2906*, Air Resour. Lab., Natl. Oceanic and Atmos. Admin., Silver Spring, Md., 1995.
- Pielke, R. A., et al., A comprehensive meteorological modeling system: RAMS, *Meteorol. Atmos. Phys.*, 49, 69–91, 1992.
- Poulet, D., Modélisation mésoéchelle de la redistribution des polluants gazeux et particulaires émis par les feux de végétation en Afrique Centrale, Comparaison avec les mesures aéroportées (Campagne EXPRESO), thèse de doct., 173 pp., Univ. de Clermont-Ferrand 2, Clermont-Ferrand, France, 2000.
- Pradelle, F., G. Cautenet, and I. Jankowiak, Remote sensing of radiative and microphysical interactions between marine stratocumulus clouds and Saharan dust, 1, Observations and climatology, *J. Geophys. Res.*, 107, 10.1029/2000JD000155, in press, 2002.
- Prospero, J. M., and R. T. Nees, Dust concentration of the atmosphere of the equatorial North Atlantic: Possible relationship to the Sahelian drought, *Science*, 196, 1196–1198, 1977.
- Pruppacher, H. R., and J. D. Klett, *Microphysics of Clouds and Precipitation*, 2nd rev. ed., Kluwer Acad., Norwell, Mass., 1997.
- Putaud, J.-P., S. Belviso, B. C. Nguyen, and N. Mihalopoulos, Dimethyl-sulfide, aerosols and condensation nuclei over the tropical northeastern Atlantic Ocean, *J. Geophys. Res.*, 98, 14,863–14,871, 1993.
- Römer, F. G., J. W. Viljeer, L. Van Den Beld, H. J. Slangeval, A. A. Veldkamp, and H. F. R. Reijnders, The chemical composition of cloud and rain water, Results of preliminary measurements from an aircraft, *Atmos. Environ.*, 19, 1847–1858, 1985.
- Schell, D., et al., The size-dependent chemical composition of cloud droplets, *Atmos. Environ.*, 31, 2561–2576, 1997.
- Schütz, L., R. Jaenicke, and H. Pietrek, Saharan dust transport over North Atlantic Ocean, *Spec. Pap. Geol. Soc.*, 186, 1981.
- Sokolik, I. N., and O. B. Toon, Incorporation of mineralogical composition into models of the radiative properties of mineral aerosol from UV to IR wavelengths, *J. Geophys. Res.*, 104, 9423–9444, 1999.
- Song, C. H., and G. R. Carmichael, The aging process of naturally emitted aerosol (sea-salt and mineral aerosol) during long range transport, *Atmos. Environ.*, 33, 2203–2218, 1999.
- Twomey, S., The influence of pollution on the shortwave albedo of clouds, *J. Atmos. Sci.*, 34, 1149–1152, 1977.
- Wobrock, W., Numerische Modellsimulation von Strahlungsnebel-situation unter Berücksichtigung spektraler Wolkenmikrophysik, Ph.D. thesis, Johannes-Gutenberg Univ., Frankfurt, Germany, 1988.
- Wurzler, S., T. G. Reisin, and Z. Levin, Modification of mineral dust particles by cloud processing and subsequent effects on drop size distributions, *J. Geophys. Res.*, 105, 4501–4512, 2000.
- Zhang, Y., The chemical role of mineral aerosols in the troposphere in East Asia, Ph.D. thesis, Univ. of Iowa, Iowa City, 1994.

G. Cautenet and F. Pradelle, Laboratoire de Météorologie Physique, Université Blaise Pascal, 24 avenue des Landais, 63177 Aubière cedex, France. (g.cautenet@opgc.univ-bpclermont)